Amirhosein Yazdanbakhsh and Ghodratollah Hashemi Motlagh*

Simultaneous effects of temperature and backbone length on static and dynamic properties of high-density polyethylene-1-butene copolymer melt: Equilibrium molecular dynamics approach

https://doi.org/10.1515/epoly-2024-0072 received July 12, 2024; accepted August 27, 2024

Abstract: Temperature and chain length play significant roles in determining the physical properties of polymer melts. In the current computational research, a molecular dynamics (MD) approach was implemented to describe the static and dynamic properties of (1) high-density polyethylene-1-butene with 120 beads in backbone (PE120) and (2) entangled high-density polyethylene-1-butene with 600 beads in the backbone (PE600). The transferable potentials for phase equilibria force fields were used for CH₂ beads in a defined initial condition. First, the equilibrium phase of the designed systems was reported with total energy and density convergency at various initial temperatures (T_0 = 450, 470, and 490 K). Also, gyration radius (R_g) and end-to-end distance (R) were calculated for the static behavior description of the two PEs. Zero-shear viscosity (η_0) , mean square displacement, and diffusion coefficient (D) were estimated to define the dynamic behavior of PE120 and PE600 systems. MD outputs predicted that 10 ns is sufficient for equilibrium phase detection inside polymeric samples. After equilibrium phase detection, $R_{\rm g}$ converged to 14.97 and 17.35 Å in PE120 and PE600, respectively (T_0 = 450 K). Furthermore, MD outputs show that temperature variation can considerably affect the time evolution of the system. Numerically, the η_0 of PE120 and PE600 converged to 49 and 168 cp at 450 K. These results of η_0 parameter as a function of temperature are an important output of MD simulations. The results predicted that η_0 decreases to 24 and 44 cp for PE120 and PE600 samples with an increase in temperature from 450 to 490 K. With the creation of the entanglements network, D reached the highest value of 2×10^{-9} m²·s⁻¹ among the designed polymeric systems. The results are in good consistency with experimental reports. It is expected that the result of this study can be used in designing improved polymeric systems for real applications.

Keywords: polyethylene, chain length, dynamic properties, entanglement effect, temperature effect, molecular dynamics simulation, TraPPE

1 Introduction

Ethylene-alpha olefin copolymers exhibit excellent properties and find a wide range of applications due to the flexibility of chain design and tailoring during polymerization. The addition of 1-butene comonomer to ethylene monomer in the polymerization reactor results in short-chain branches (SCBs) of ethyl on the polyethylene (PE) backbone (1). The number, density, and distribution of these SCBs can strongly influence the physical and dynamic melt properties of PE (2). Chain entanglements significantly influence the melt properties, particularly zero-shear viscosity (η_0) of PE. This parameter in PE melt-based systems is crucial for understanding their flow behavior under processing conditions. η_0 influences the material's processing efficiency, product quality, and performance in applications. η_0 calculations provide insights into molecular interactions and entanglements, affecting how PE behaves during extrusion and molding. By analyzing these viscosity results, manufacturers can optimize processing parameters, enhance material properties, and predict performance in end-use applications, ultimately

Amirhosein Yazdanbakhsh: Polymer Engineering Group, School of Chemical Engineering, College of Engineering, University of Tehran, P.O. Box 11155-4563, Tehran, Iran

^{*} Corresponding author: Ghodratollah Hashemi Motlagh, Polymer Engineering Group, School of Chemical Engineering, College of Engineering, University of Tehran, P.O. Box 11155-4563, Tehran, Iran, e-mail: ghmotlagh@ut.ac.ir

leading to better product design and reduced production costs (3). When the backbone length is sufficient to form entanglements, segmental motions, and consequently, the dynamic properties of the chains will differ before and after entanglement (4). Therefore, it is important to study the dynamic behavior of PE chains above entanglement molecular weight (M_e) . η_0 experiences a large increase at M_e . Investigating the physical and dynamic behavior of the chains beyond this weight is of paramount importance (5). In thermodynamic equilibrium, temperature plays a crucial role in the melt behavior of PE, and temperature variations induce changes in the dynamics of the PE chains. Additionally, the dependence of the dynamic diffusion coefficient (D) on temperature is considered one of the most important variables in the equilibrium of PE melt. At equilibrium, the activation energy of PE signifies the temperature dependence of D (6,7).

Simulating the melt flow of PE provides useful and applied information for its processing. The melt processability of PE is strongly influenced by its structure, molecular weight and physical properties (8). As a result, recent investigations into the melt behavior of PE have garnered attention, particularly for entangled chains and branched molecular architectures (9,10). Molecular dynamics (MD) approach is an interesting and adequate method for studying the physical behavior of PE due to its ease of application and its ability to provide direct and effective information on the evolution of physical and dynamic properties over time (11,12). Therefore, given that simultaneous oscillatory movements of atoms and segmental motions occur in the PE chain, selecting a very short time step and a high number of steps in MD simulation is essential. To address this limitation, the use of coarse-grained models, including bead-spring models, is common to achieve satisfactory simulation times (13). Many coarse-grained models consider CH, CH₂, and CH₃ groups as unified carbon atoms when describing the melt behavior of PE (14,15). η_0 can be directly calculated in equilibrium MD simulations using the time integral of the stress tensor components (16).

The study by Harmandaris et al. (17) stands out as one of the earliest research endeavors exploring the dynamic properties of PE melt through MD simulation. They simulated linear PE melt under equilibrium conditions using the MD method. Additionally, they employed the Rouse model to calculate friction and diffusion coefficients and η_0 for various chain lengths of PE, both below and above the entanglement molecular weight. They compared these calculations with the results of experimental studies. They showed that η_0 and D are strongly correlated with backbone length. In a MD simulation by Padding and Briels (5) in coarse-grain mode, linear PE melt with backbone lengths ranging from 80 to 1,000 carbon atoms was examined under equilibrium conditions for structural and dynamic analysis.

Each set of 20 carbon atoms was considered as one bead in this simulation. The results indicated an expected increase in the average mean square gyration radius (R_g^2) and mean square end-to-end distances (R) of the chains. Another significant outcome of this research was reporting η_0 values within the range of entanglement molecular weight and critical molecular weight (M_c) . In another study, Ramos et al. (18) investigated the effect of short branches on the equilibrium melt dynamics of linear PE with 1,000 united atoms in the main chain using MD simulation. They calculated the melt density of PE with varying percentages of SCBs, 1.9–11.5%, in the range of 0.770–0.775 g·cm⁻³. Additionally, an increase in the average square of R with an increase in the number of bonds in the main chain was confirmed. In their subsequent research, Ramos et al. (19) examined the structure and dynamics of linear PE above the entanglement molecular weight using MD simulation. Considering the simulation results, they discussed mesoscopic properties such as density, physical parameters like the characteristic ratio (C_{∞}) , static chain features such as $R_{\rm g}$, and dynamic properties such as D.

In the present study, PE chains with 120 and 600 numbers of CH2 beads in the backbone containing varying amounts and distributions of SCBs of ethyl are modeled. The temporal transformations of the system are investigated at molecular weights above the entanglement molecular weight and above the critical molecular weight at different temperatures. Most MD simulation studies conducted on the structure and dynamics of molten PE so far have either modeled its linear structure, examined the modeled system's transformations below the critical molecular weight, or been limited to a constant temperature. The present improved MD simulations investigate the dynamic behavior of PE melt in the presence of chain entanglements as a function of temperature, which shows good compatibility with experimental results. So, the current research introduced the effect of molecular weight and temperature parameters on valuable physical properties of the molten PE samples (such as $R_{\rm g}$, D, and η_0) with particle-based simulations for the first time. A united atomic structure suitable for the studied branched copolymer was developed then an appropriate force field was used to create thermodynamic equilibrium. The melt density, static and dynamic parameters of PEs at two MWs, and varying content and distribution of SCBs and three temperature levels were calculated. Subsequently, structural and static transformations of the modeled copolymer chains were evaluated by calculating $R_{\rm g}$, interaction/total energies, and R parameters. Furthermore, the melt dynamics of PE was studied by calculating properties such as η_0 , mean square displacement (MSD), and D for the produced structures at three temperature levels.

2 MD details and molecular samples

 $M_{\rm e}$ at which chains start to entangle is defined in the literature as 1,680 g·mol⁻¹ or 120 beads (CH₂) (20). M_c at which the slope of zero shear viscosity vs MW increases from 1 to 3.4 is defined in the literature as 5,000 g·mol⁻¹ or 357 beads (CH₂) (5). In current computational research, the time evolution of branched PE above M_e and M_c was described using the MD approach. Polymer chains were modeled as CH₂ and CH₃ units or united beads. Two various types of chains including 120 and 600 beads were modeled inside the computational box as depicted in Figure 1. Polymeric chains were randomly modeled inside computational boxes using PACKMOL software (21). A minimum distance of 2 Å was set to prevent unactual bonds between polymer chains. Also, a branching degree was set to 1.7% and 1% (22) for the ethyl branch was assigned. The initial temperature was set to 450, 470, and 490 for 15 ns. The large-scale atomic/molecular massively parallel simulator (23) package, released by Sandia National Laboratory, was used in the simulations.

2.1 MD method

MD simulation is a powerful computational method to study the behavior of molecules and atoms over time. In the context of polymeric structure studies, MD simulations are particularly valuable for investigating the dynamic properties and structural characteristics at the molecular level.

In a polymeric system, MD simulations involve representing a polymer chain as a series of connected beads (representing repeating atomic units) interacting with each other through an interatomic force field (potential function).

Newton's law is computationally implemented between beads (24),

$$F(X) = -\nabla E(X) = M\dot{V}(t) \tag{1}$$

$$V(t) = \dot{X}(t) \tag{2}$$

where F is the interparticle force, which is described by potential function (E), X and V are the position and velocity of each particle, respectively, with M being mass. These computational functions describe the forces between beads and are used to calculate the motion of the beads over time. In the current research, the Transferable Potentials for Phase Equilibria (TraPPE) force field (25,26) was used to define inter-beads interaction. According to previous investigations, this force field has a better numerical decision rather than other types for PE physical performance description (19). In this force field, the non-bond interaction (27) is described with Lennard-Jones (LJ) potential (28) according to the following equation:

$$E_{\rm LJ} = 4\varepsilon \left[\left(\frac{\sigma}{r} \right)^{12} - \left(\frac{\sigma}{r} \right)^{6} \right], \quad r < r_{\rm c}$$
 (3)

Here, ε and σ represent the energy and distance parameters, respectively. r_c defines the cutoff radius in the LJ equation. The energy of simple and angular bonds are described according to the following equations:

$$E_{\rm b} = K_{\rm b}(r - r_0)^2 \tag{4}$$

$$E_{\rm a} = K_{\rm a}(\theta - \theta_0)^2 \tag{5}$$

where $K_{\rm b}$ and $K_{\rm a}$ are harmonic constants and r_0 and Θ_0 represent equilibrium distance and angle, respectively. Finally, the dihedral interactions are defined with "n-harmonic" relation according to the following equation (29):

$$E_{\rm d} = \sum_{i=1,m} A_i \cos^{i-1}(\varnothing) \tag{6}$$

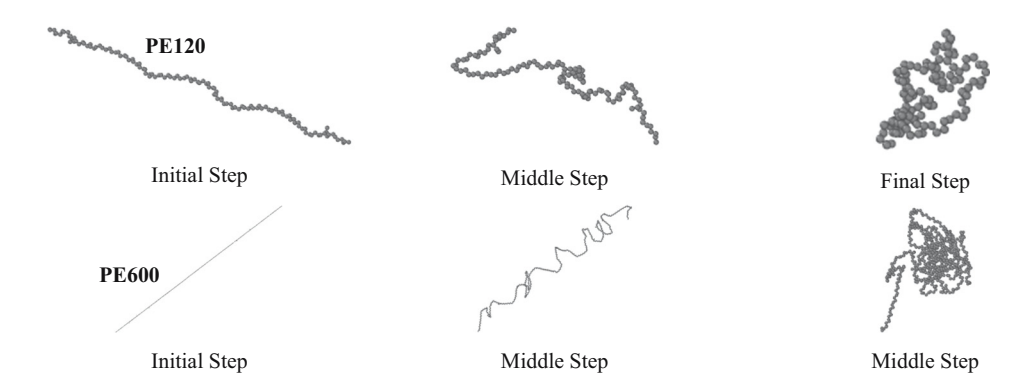


Figure 1: Structural evolution of PE120 and PE600 chains in the modeling phase of current computational research. These graphical outputs were created using OVITO (35) software.

where A and \emptyset are the amplitude and angle of the angular oscillator, respectively. In the selected force field, m parameter is set to 9. After force field definition, Newton's equation is solved, and new positions/velocities of each bead are estimated. Technically, this process has a high computational cost. Various algorithms have been proposed to solve this problem. Among them, the velocity-Verlet algorithm as an effective method was selected (30) using the following equations:

$$X_{i+1} = X_i + V_i \Delta t + \frac{1}{2} a_i \Delta t^2 = X_i + \Delta t \left(V_i + \frac{1}{2} a_i \Delta t \right)$$
 (7)

$$V_{i+1} = V_i + \frac{1}{2}(a_i + a_{i+1})\Delta t$$
 (8)

where X_i and V_i parameters define the position and velocity of the ith particle. Δt and a represent timestep and acceleration, respectively. Through MD simulations, it can be observed how polymer chains move, interact, and arrange themselves in different initial conditions, here, in various temperatures. This provides insights into properties such as chain configuration, dynamic behavior, and thermodynamic properties of modeled PE-based systems.

2.2 Details of MD simulations

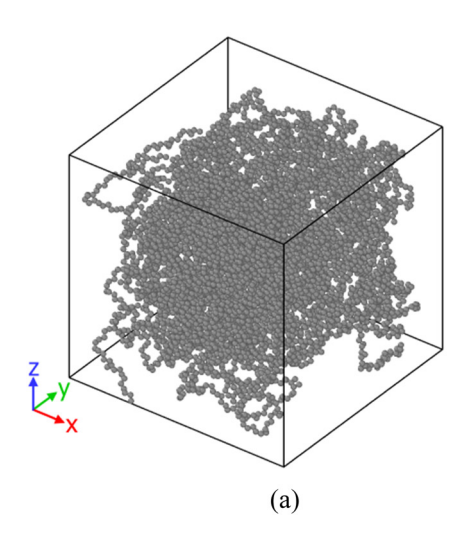
The MD simulations in this work are done in equilibrium conditions. The initial pressure was set to 1 atm, and the initial temperature was set to 450, 470, and 490 K using the Nose Hoover algorithm (31). A temperature/pressure damping value of 1/100 fs was set to reach the equilibrium phase.

Several parameters, such as total energy and temperature variation as a function of simulation time, are reported after reaching the equilibrium phase (after 10 ns). Furthermore, physical outputs such as interaction energy, density, MSD, D, η_0 , R_g , and R are calculated to report static and dynamic behavior of PE-based systems (5 ns later of equilibrium phase detection).

3 MD simulation results

3.1 Equilibrium phase and validation of modeled polymeric samples

In the first step of current computational research, the equilibrium phase of the designed polymeric systems is reported. The atomic arrangements of the equilibrated



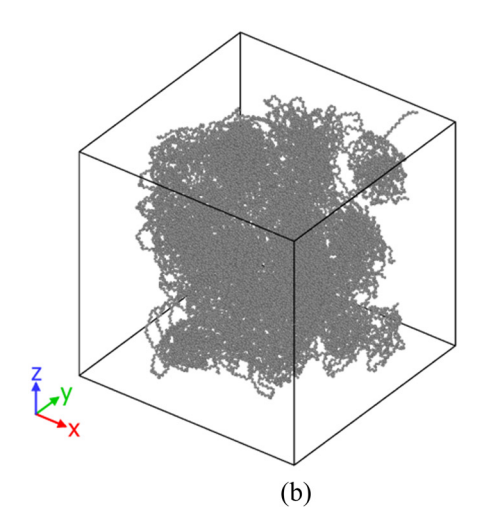


Figure 2: Graphical representation of (a) simulation box in the presence of 60 chains of PE120 and (b) simulation box in the presence of 60 chains of PE600.

Table 1: MD simulations settings in current computational research

Computational parameter	Value/setting
Box size	65 × 65 × 65 Å ³ (for PE120 sample) 150 × 150 × 150 Å ³ (for PE600 sample)
Number of total beads	7,440 (for PE120 sample) 36,720 (for PE600 sample)
Temperature	450, 470, and 490 K
Pressure	1 atm
Damping of temperature	1 fs
Damping of pressure	100 fs
Timestep	1 fs
Total simulation time	15 ns

matrix with 60 chains of polyethylene-1-butene with 120 (PE120) at varying temperatures are shown in Figure 3. The MD outputs showed that the temperature of the systems converged to 453.958, 476.921, and 493.154 K after 10 ns. Physically, these convergencies show that the amplitude of atomic fluctuations decreases by simulation time. The total energy parameter is appropriate to analyze this atomic evolution. The numerical results for the total energy parameter are reported in Figure 4. The total energy normalized to the bead numbers for the PE120 matrix was converged to 29.860, 29.994, and 30.053 kcal·mol⁻¹ at 450, 470, and 490 K, respectively. The total energy convergency in this computational step indicates that the attraction forces between various particles are developed for the applied initial condition. So, it is expected that structural stability occurs after 10 ns inside the MD box.

The polymeric matrix, which was designed by 60 chains of PE600, shows similar equilibrium behavior as

Table 2: TraPPE force field coefficients in current research

Parameter	Value
ε	0.0914 kcal·mol ^{−1}
σ	3.95 Å
r_{c}	9.085 Å
\mathcal{K}_b	95.88 kcal·mol ^{−1}
r_0	1.54 Å
K _a	62.1 kcal·mol ^{−1}
Θ_0	114°
A_0	1.9892 kcal·mol ^{−1}
A_1	4.2328 kcal·mol ⁻¹
A_2	−0.6021 kcal·mol ^{−1}
A_3	−7.1778 kcal·mol ^{−1}
A_4	4.4255 kcal·mol ⁻¹
A ₅	3.9068 kcal⋅mol ⁻¹
A_6	−8.9206 kcal·mol ^{−1}
A_7	−3.4498 kcal·mol ^{−1}
A_8	5.5980 kcal·mol ⁻¹
m	9

reported before for PE120. As shown in Figure 5, the appropriate structural unity can be seen in the PE600 matrix at various temperatures. These structural unities arise from atomic interactions in various initial conditions. Numerically, the total energy/bead of PE600 matrix converged to 32.862, 33.013, and 33.152 kcal·mol⁻¹ at 450, 470, and 490 K, respectively (Figure 5d). These energy outputs predicted that the PE600 matrix can be stabilized in actual applications.

The detection of the equilibrium phase was a qualitative validation for the computational method. To quantitatively validate the simulation method, the variation of melt density with simulation time at three temperatures is shown in Figure 6a for the PE120 matrix. In this figure,

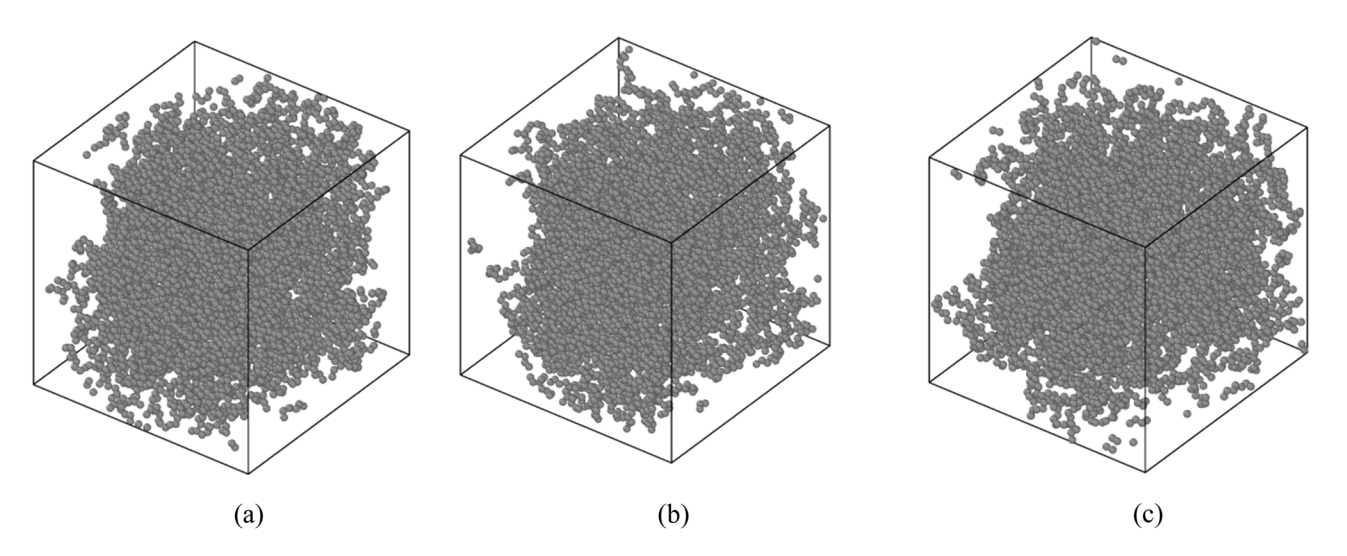


Figure 3: Structure of the PE120 matrix arrangement after equilibrium phase detection at (a) 450, (b) 470, and (c) 490 K.

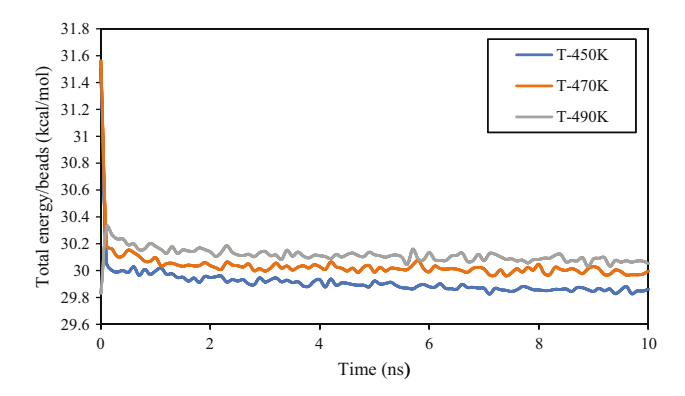


Figure 4: Total energy/bead parameter changes as a function of initial temperature in the modeled PE120 matrix.

the melt density of the system converges to 0.732, 0.716, and 0.700 g·ml⁻¹ at 450, 470, and 490 K, respectively, which are in agreement with previous reports (18). The reported density convergencies arise from the change of volume from 274,625 to 230,688.52 Å³ as listed in Table 3. Physically, an increase in thermal energy increases the mean distance

between the beads and, therefore between the chains, which increases the volume and decreases the density of the system.

Furthermore, Figure 6b presents the melt density of the PE600 matrix at the mentioned temperatures. Numerically, the density of PE600 converged to 0.855, 0.823, and 0.812 g·ml⁻¹ for the initial temperatures of 450, 470, and 490 K. The decrease in density with temperature is in agreement with the experimental results (5,18,33). Alnaimi et al. (36) reported that the density of the PE-based system changed with 0.01 g·ml⁻¹ by 20 K enlarging in temperature value. This numeric output is consistent with our work. For the PE600 system in which chain MW is well above $M_{\rm c}$, the entanglement network is established, attraction forces between various chains are intensified, and the packing ratio increases. Therefore, it is seen that density values are considerably higher than those values of PE120. As reported in Table 3, the volume changes in the PE600 matrix vary from 3,375,000 to 2,371,906.82 Å^{3,} which is much wider than that for PE120.

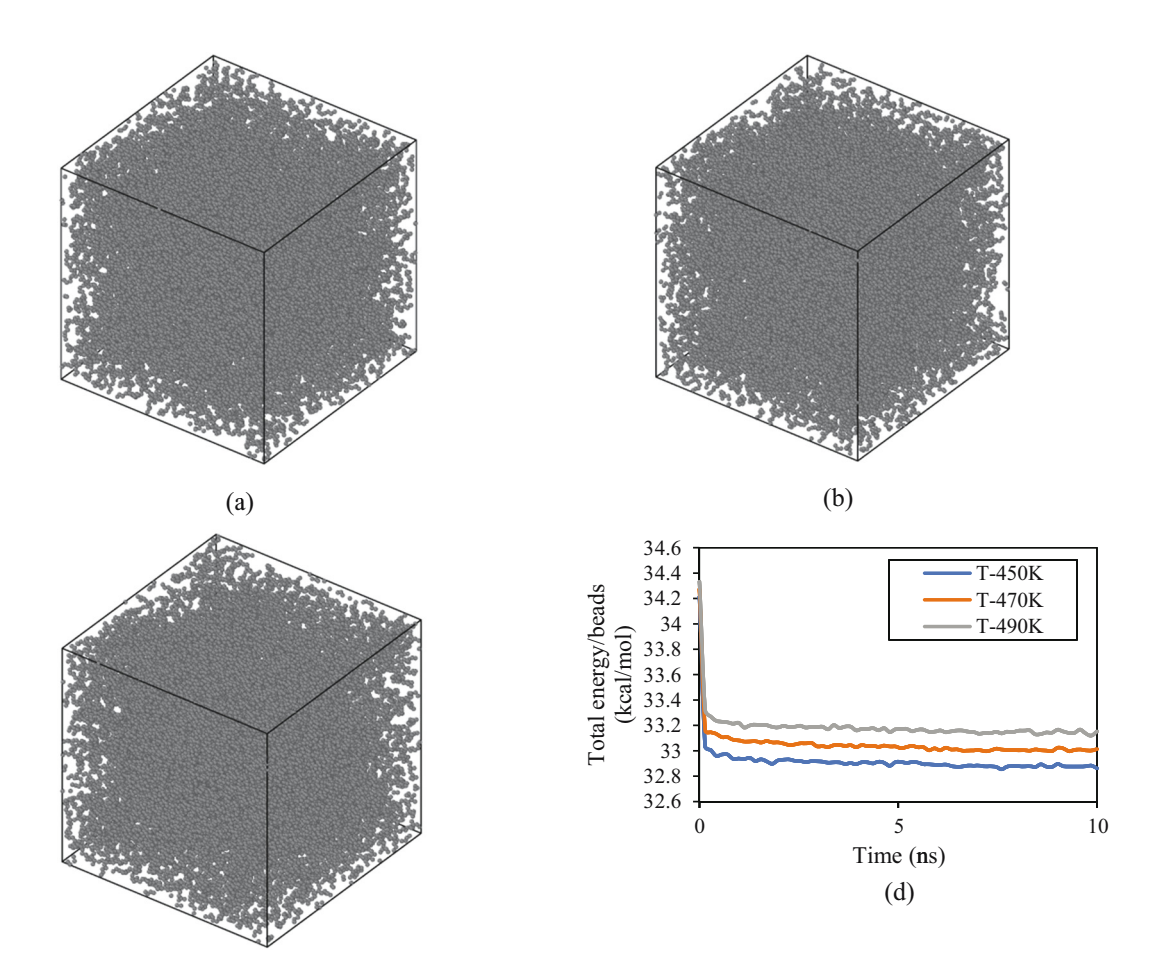


Figure 5: Structure of the PE600 matrix arrangement after 10 ns at (a) 450, (b) 470, and (c) 490 K. (d) (Total energy)/(beads) changes as a function of initial temperature in the PE600 sample.

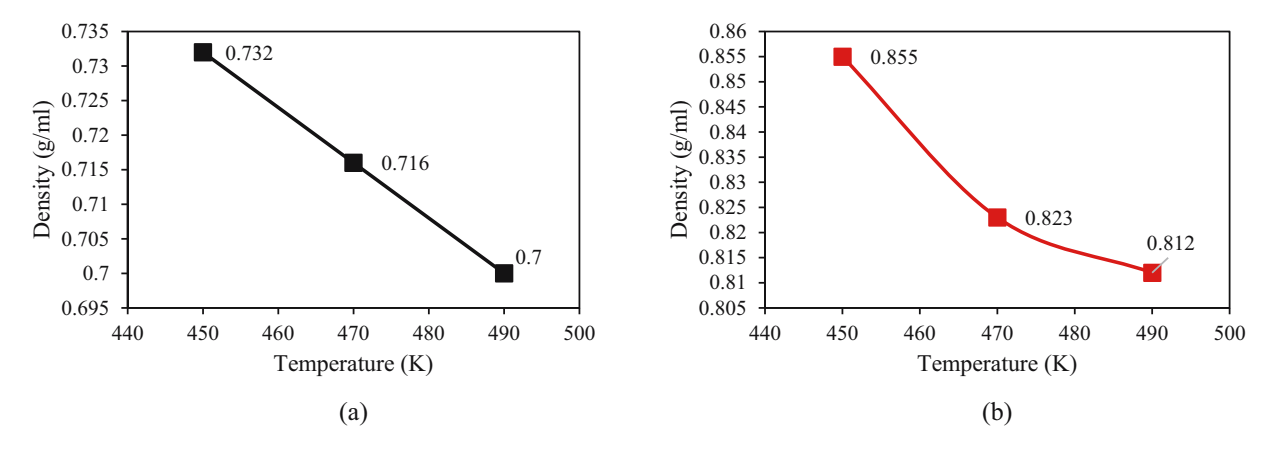


Figure 6: Density changes as a functional initial temperature after 10 ns for (a) PE120 and (b) PE600 matrices.

Table 3: Density and volume changes (ΔV) in various modeled polymeric matrices

Matrix-temperature	Density (g·ml ⁻¹)	$\Delta V (\hat{A}^3)$
PE120-450 K	0.732	-38,404.96
PE120-470 K	0.716	-33,425.67
PE120-490 K	0.700	-43,936.48
PE600-450 K	0.855	-2,371,906.82
PE600-470 K	0.823	-2,336,978.04
PE600-490 K	0.812	-2,325,898.16

The described density convergency can be analyzed by the radial distribution function (RDF) parameter (Figure 7). This parameter in polymeric systems describes the probability of finding a bead at a certain distance from a reference one within the polymer chain (37). It provides insights into the spatial arrangement and organization of monomers within the polymer structure, reflecting the polymer's local ordering and packing characteristics. By analyzing the peaks of various designed structures, it is concluded that these peaks occur in the vicinity of r = 1.5 Å. Furthermore, MD

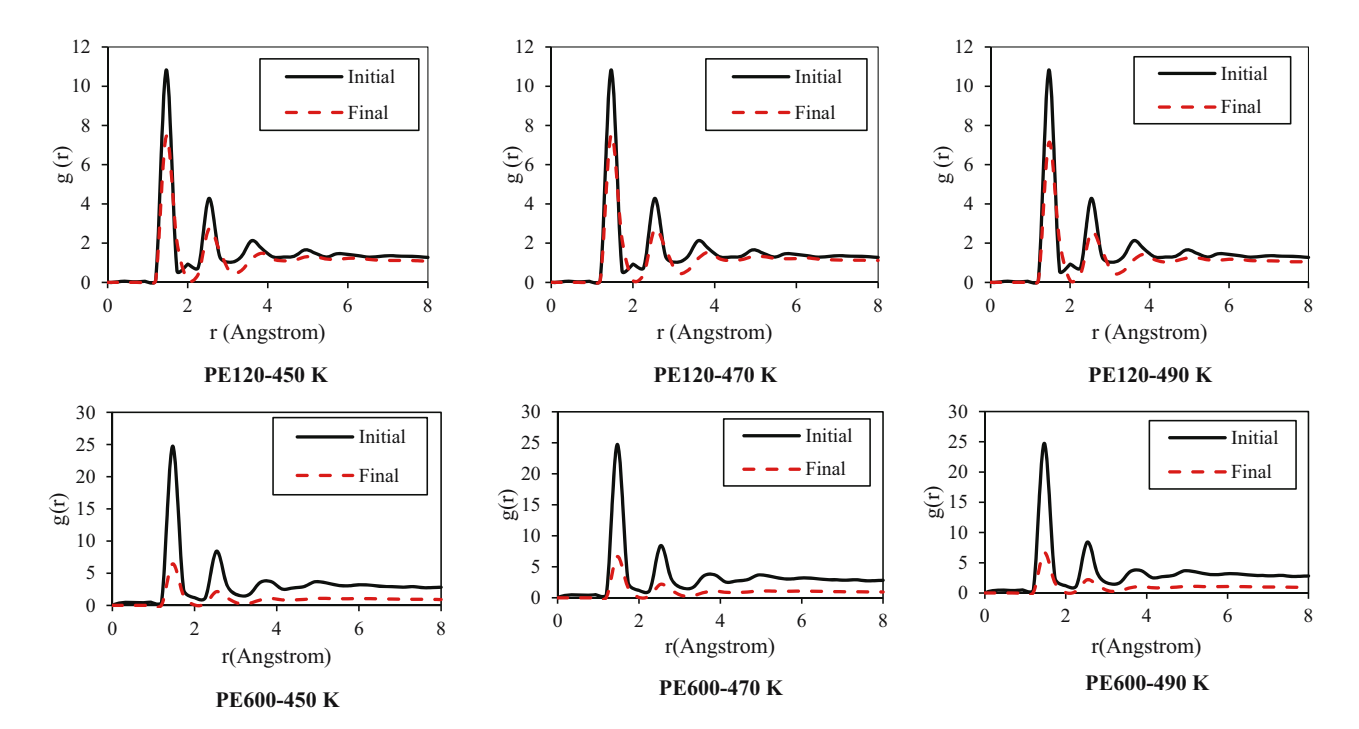
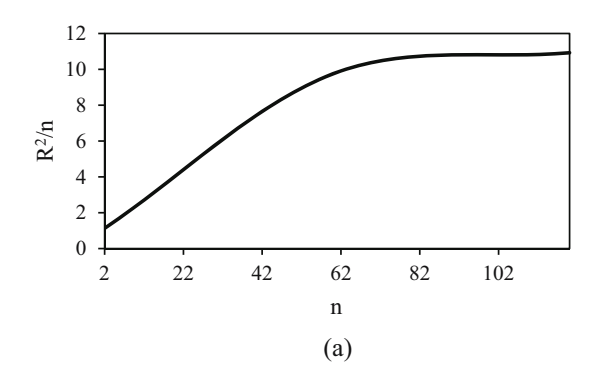


Figure 7: RDF in the initial and final time step of designed polymeric matrices at various temperatures.



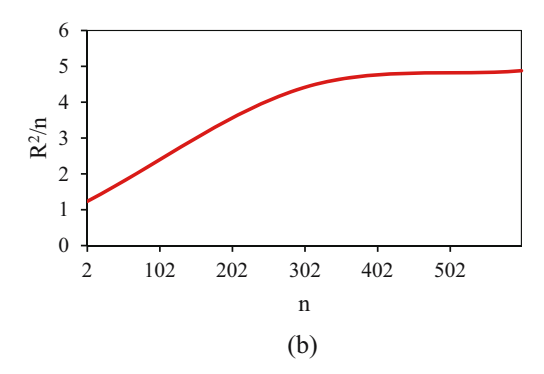


Figure 8: R_n^2/n changes as a function of *n* parameter for (a) PE120 and (b) PE600 matrices at 450 K.

outputs show that the RDF peak values, g(r), decrease for the PE120 matrix with MD runtime. This structural evolution predicted the polymeric chains' mean distance converge to a larger value. Similarly, in PE600, g(r) values decreased in the final time step (10 ns) in comparison to the value at the initial timestep with higher intensity than the value for the PE120 system. It is most likely that the network formation of entanglements above M_c has caused this considerable structural behavior for PE600 as compared to PE120.

In MD simulation of polymer-based systems, the total energy and density convergencies over simulation time are necessary but insufficient. Therefore, to ensure the sufficiency of simulation time to detect the equilibrium phase, the convergence of R_n^2/n against n is evaluated (33). R_n is

the distance between bead number 1 and bead number n. The convergencies of this parameter (R_n^2/n) as a function of n at 450 K are shown in Figure 8. The curves had a similar pattern at 470 and 490 K as well.

3.2 Structural properties of modeled polymeric matrices

MD simulation results showed that 15 ns is the sufficient time to detect the final arrangement of beads in designed polymeric systems. In Figure 9, the RDF of various samples was depicted. This structural output indicated their

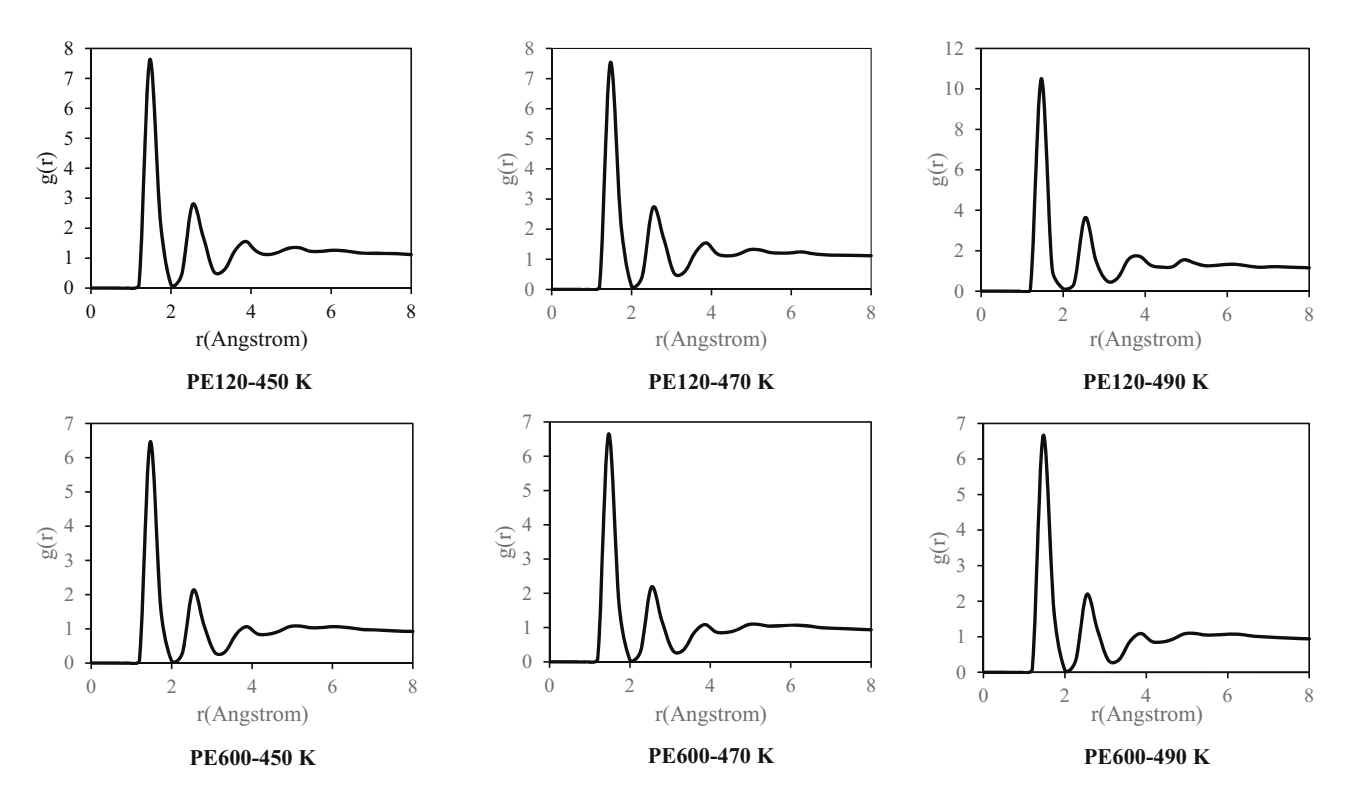


Figure 9: RDF of designed polymeric matrices at various temperatures after 15 ns.

The distance between the ends of a polymer chain, R or

end to end distance, is an important property of a polymer chain to understand the physical properties and behavior of polymer chains in defined condition. To calculate this parameter, several chains were selected from various regions of the box and their average end-to-end distance was assigned as *R*. The change of *R* with temperature is shown in Figure 11. A monotonic change is not observed for

Table 4: Structural details and potential energy of the designed polymeric matrix with modeled PE600 in current research after 15 ns

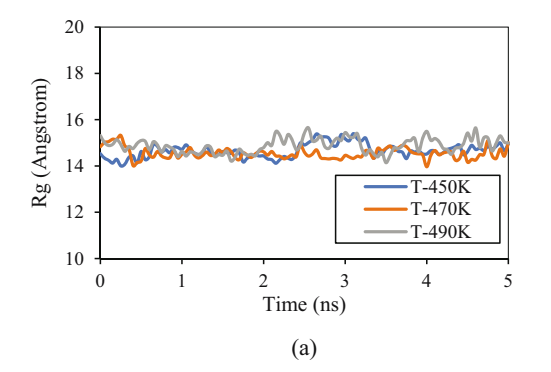
Matrix- temperature	Initial box length (Å)	R _g (Å)	R (Å)	C_{∞} $(\frac{R^2}{nr_0^2})$ (42,48)	Potential energy/ beads (kcal·mol ⁻¹)
PE120-450 K	65	14.973	37.910	10.646	28.508
PE120-470 K	65	15.004	37.364	10.341	28.551
PE120-490 K	65	14.991	38.242	10.833	28.624
PE600-450 K	150	17.167	54.100	4.336	31.526
PE600-470 K	150	17.000	47.990	3.411	31.602
PE600-490 K	150	17.343	43.970	2.860	31.667

stability. Furthermore, the potential energy of each PE-based system converged to a constant value in the final time step, as listed in Table 4. This energy convergency arises from the mean attraction force between chains in various regions of the MD box. $R_{\rm g}$ in polymeric systems is a measure that describes the average size of a polymer chain. It represents the average distance between the center of mass of the chain and its individual constituents. $R_{\rm g}$ is an important property for understanding the conformation and physical properties of polymer melts. Compu-

tationally, this parameter is calculated with $R_{\rm g} = \sqrt{\left(\frac{\sum_{i=1}^n m_i \mathcal{E}_i^2}{\sum_{i=1}^n m_i}\right)^2}$

(38). Here, δ is particle distance for the center of mass. In polymeric systems, R_g is influenced by various factors such as chain length, chain structure, intermolecular interactions, and melt conditions. Figure 10 shows R_g values for PE120 and PE600 matrices against initial temperature. A larger R_g indicates a more elongated chain, while a smaller R_g suggests a more compact conformation (39). Numerically, R_g changes from 14.973 to 15.004 Å in the PE120 matrix in the temperature range of the study. Comparatively, it changes from 17.346 to 17.935 Å in PE600. The rate of change in R_g with chain length in this work is also in agreement with experimental results (40).

R against temperature for PE120 but it is decreasing for PE600. R was used to calculate C_{∞} parameter, which is an indication of chain rigidity. C_{∞} values of 10.833 and 4.336 were obtained for PE120 and PE600, respectively (Figure 11), which are in agreement (5,000 g·mol⁻¹ (5)) with previous simulation and experimental data (19,41,42). Numerically, this parameter changed by temperature enlarging and converged to 38.242 from 37.910 Å in the PE120 matrix. This behavior arises from atomic fluctuation intensity enlarging in higher temperatures. This atomic evolution can be described by $\frac{1}{2}mv^2 = \frac{3}{2}KT$ relation (43). MD outputs in this section of computational research are consistent with $R^2 = 6R_g^2$ experimental relation. In current simulations, the R^2/R_g^2 parameter was converged to about 6 values after 15 ns. The result of this computational step is consistent with previous studies (18). Furthermore, the number of the beads increasing inside chains caused the R parameter to enlarge to 54.1 Å in the PE600 matrix. In large polymeric chains, the volume of beads distribution gets to a higher volume. So, this structural property caused the R parameter to increase in this modeled sample. Note that intensifying of entanglement network creation in larger temperatures is crucial. In the PE600 sample, temperature convergency to 490 K caused the limitation in beads evolution by time passing which arises from entanglement network creation with more intensity. So, this behavior caused to decrease of the R parameter with temperature enlarging (converse to PE120 sample structural behavior). 20 18



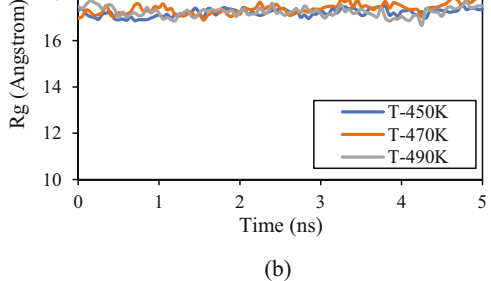


Figure 10: Rg parameter changes as a function of the MD simulation time for (a) PE120 and (b) PE600 matrices in various initial temperatures.

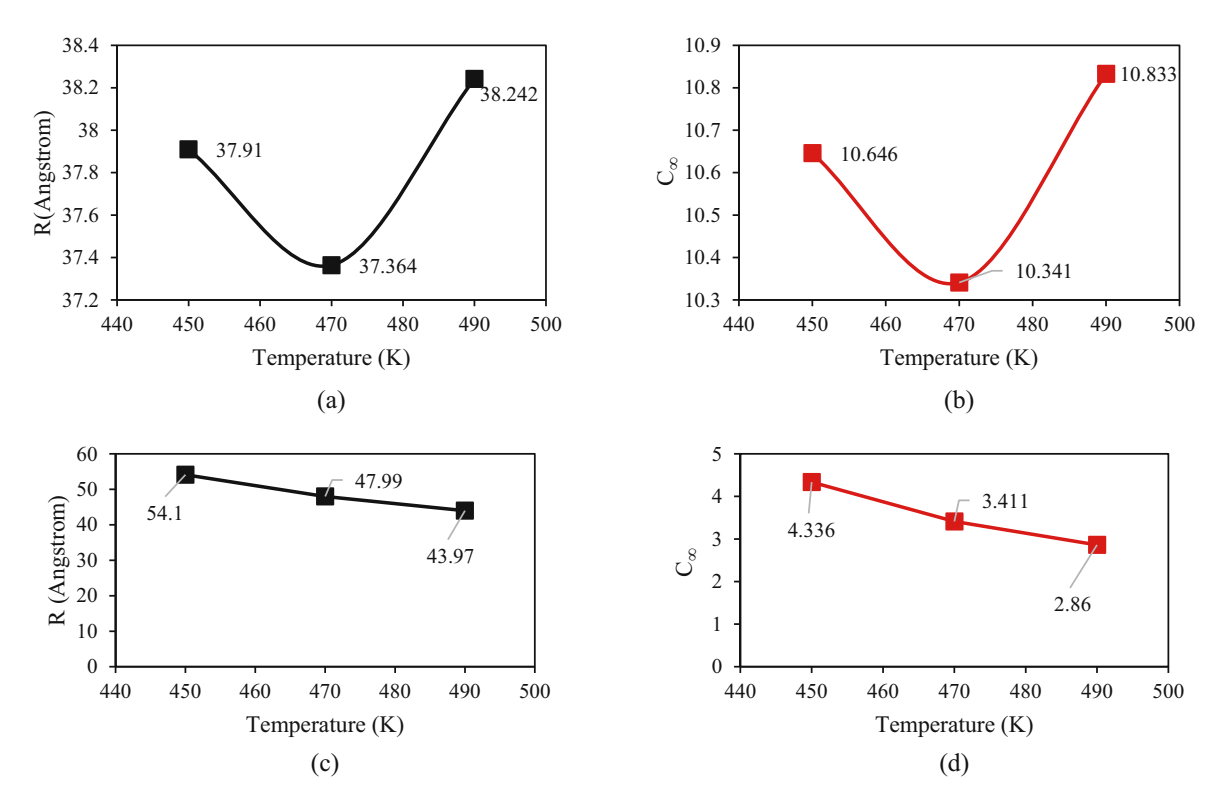


Figure 11: (a) R and (b) C_{∞} of PE120 matrix variations in different temperatures after 15 ns. (c) R and (d) C_{∞} of PE600 matrix variations in different temperatures after 15 ns.

The stability of structural performance and R parameters can be analyzed with total energy inside designed polymeric samples. This parameter plays a crucial role in describing the interactions between polymer chains. Total energy defines the energy associated with stretching, bending, and torsional movements within the polymer chains, as well as the interactions between different chains (41). MD outputs for total energy changes as a function of simulation time for the PE600 sample depicted in Figure 12a. From this figure, the energy/bead parameter converged to 32.855, 33.012, and 33.138 kcal·mol⁻¹ at 450, 470, and 490 K, respectively. These convergencies arise from polymeric chain mobility restriction in defined conditions. Also, interaction energy value shows similar behavior as depicted in Figure 12b. This energy/bead parameter reached negative values after 15 ns $(-0.778, -0.752, and -0.741 \, kcal \cdot mol^{-1}$ at 450, 470, and 490 K, respectively). These negative values predicted the mean attractive force between beads in modeled systems (44,45). These calculated energies predicted the mean distance between polymeric chains in various regions of polymeric samples to get a lesser ratio by MD time passing. The C_{∞} of a polymeric system after entanglement network creation has a lesser value due to the mobility of each beads increased, and this structural evolution caused the flexibility of each chain to be enlarged in defined conditions (46). On the other hand, when polymer

chains become entangled with higher intensity (in the presence of a large number of monomers), they experience high attraction force. This behavior caused the conformational flexibility (47). In the current case study, the effect of the first phenomenon has more effect on the structural evolution of the PE600 system, which should be supposed in actual application. All structural properties of modeled systems are reported in Table 4.

3.3 Dynamical properties of modeled polymeric matrices

In polymeric systems, MSD is a measure of the average squared distance that individual polymer segments or molecules move over time. It provides insight into the self-diffusion and mobility of polymeric chains within the modeled matrices. By analyzing how the MSD changes with time, researchers can characterize the dynamics of polymers, including their flexibility, entanglement, and overall motion. Computationally, this parameter is calculated by the average of $(r(t) - r(0))^2$, where r(t) is the position of the particle at time t and r(0) is its initial position (49). Figure 13 shows the MSD outputs for PE120 and PE600 at various

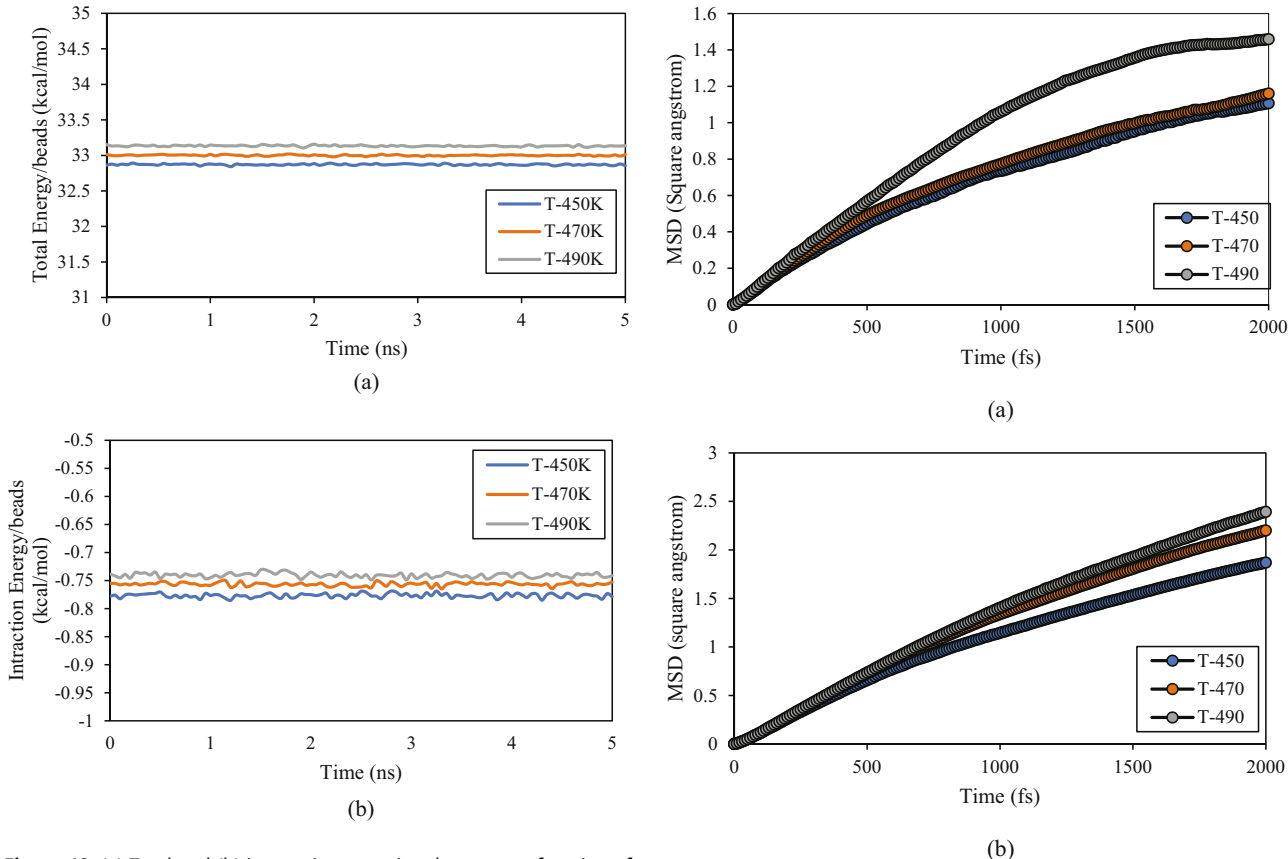


Figure 12: (a) Total and (b) interaction energies change as a function of MD simulation time in modeled PE600 matrices.

Figure 13: Linear section of MSD parameter vs MD time for (a) PE120 and (b) PE600 at varying temperatures.

temperatures. It is seen that MSD increases with temperature due to the increase in thermal energy and further movement and fluctuations of the segments (50). Also, MSD of PE600 is more than twice higher than PE120 since it is well known that MSD increases with chain length (47). This atomic evolution predicted the MSD of PE120 to reach 1.459 Ų at 490 K. Furthermore, the D parameter can be calculated with the equation $D = \lim_{t \to \infty} \frac{\text{MSD}(t)}{6t}$ (48). Table 5 gives the values of D calculated from MSD changes in the first linear region of the curve. The values of D are in a range from 0.833 to 1.333 (×10⁻⁹ m²·s⁻¹) at varying temperatures for PE120, which are consistent with the previous reports (51,52). In their report, the D parameter is

of order 10⁻⁹ m²·s⁻¹. MD simulation time for MSD calculations was continued to 5 ns to obtain MSD in infinite time. The maximum value in Figure 14 shows that MSD of PE600 extends beyond 50 Å² (47). Computationally, results for MSD as a function of temperature and polymeric system types were shown in the PE120 sample affected by temperature increasing with lesser intensity. This structural performance arises from a low number of beads in this type of designed sample. Instead, the temperature enlarging was affected appreciably by the mobility in PE600-based systems. The high number of beads in PE600 caused this mobility to

Table 5: Diffusion coefficient D of PE120 and PE600 at varying temperatures matrices after 15 ns in comparison with D values from the Rose model

Temperature (K)			D (×10 ⁻⁹ m ² ·s ⁻¹)	
	PE120	PE600	$\frac{1.65}{M_{ m W}^{1.98}}$ (PE120-PE600)	Rose model (PE120-PE600)
450	0.83	1.5	0.06-0.003	0.03-0.06
470	0.92	1.83	NA	0.03-0.05
490	1.33	2.00	NA	0.03-0.04

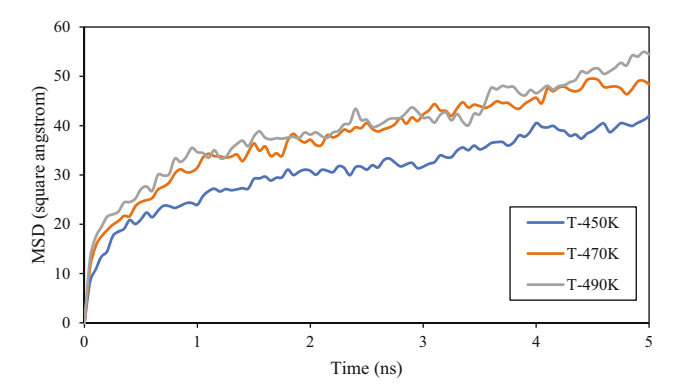


Figure 14: Extended curve of MSD vs MD time for PE600 matrix.

increase by low temperature enlarging inside the computational box.

The *D* parameter obtained from MSD calculations deviates from the Rouse model ($D = \frac{R^2}{3t\pi^2}$). Such difference has already been addressed for molten PE matrices, attributing it to factors such as the short length of modeled chains and the neglect of intermolecular forces in the Rouse model (53). As expected, the deviation from the Rouse model decreases with increasing chain length. For PE600, the *D* parameter varies from 1.5 to 2 (×10⁻⁹ m²·s⁻¹) with temperature. These results are consistent with the findings of previous reports (51,52) by experimental and simulation techniques. Ramos et al. (51) introduced 10^{-15} – 10^{-9} m²·s⁻¹ interval value for *D* parameter of their modeled PE-based samples. Furthermore, Huster et al. (52) reported 2.3 (×10⁻⁹ m²·s⁻¹) for the PE system from their experimental method. Also, Pearson et al. (54) proposed that $D = \frac{1.65}{M_w^{1.98}}$ (cm²·s⁻¹) relation for *D* parameter using this approach.

In summary, higher temperatures facilitate more energetic collisions of polymer chains, enabling them to overcome barriers and move more freely within the polymeric system. This increased mobility at elevated temperatures leads to a higher self-diffusion coefficient for the bead-base model. From diffusion coefficient outputs and previous experimental results, the $E_{\rm a}$ parameter can be calculated using $E_{\rm a}-E_{\rm a0}=\ln{(D/D_0)}\times R(T-T_0)$ relation (6). Here, $E_{\rm a}$ and D parameters define activation energy and diffusion coefficient (55), respectively. Using the D values of Table 5, ΔE ($E_{\rm a}-E_{\rm a0}$) is estimated as less than 1 kcal·mol⁻¹ when initial temperature varies from 450 to 490 K (consistent with ref. (6)).

In the final step of the current research, η_0 of various modeled structures was calculated. For this purpose, the "Green–Kubo" approach (56) as an equilibrium MD method was implemented. Here, the ensemble average of the autocorrelation of the stress/pressure tensor was used to calculate the viscosity. Furthermore, the stress tensor for each bead is given by the following formula,

$$S_{ab} = -mv_a v_b - W_{ab} \tag{9}$$

where S_{ab} is the stress tensor, mv_av_b is the kinetic energy contribution for bead i, and W_{ab} is the virial contribution due to inter-beads interactions obtained from Eq. 9.

$$W_{ab} = \frac{1}{2} \sum_{n=1}^{N_{p}} (r1_{a}F1_{b} + r2_{a}F2_{b}) + \frac{1}{2} \sum_{n=1}^{N_{b}} (r1_{a}F1_{b} + r2_{a}F2_{b})$$

$$+ \frac{1}{3} \sum_{n=1}^{N_{a}} (r1_{a}F1_{b} + r2_{a}F2_{b} + r3_{a}F3_{b})$$

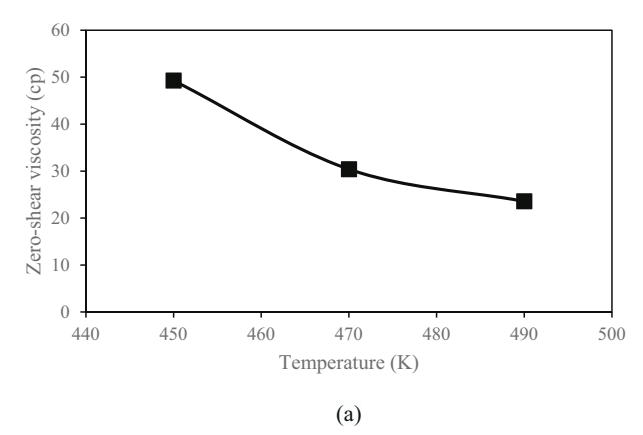
$$+ \frac{1}{4} \sum_{n=1}^{N_{d}} (r1_{a}F1_{b} + r2_{a}F2_{b} + r3_{a}F3_{b} + r4_{a}F4_{b})$$

$$+ \frac{1}{4} \sum_{n=1}^{N_{i}} (r1_{a}F1_{b} + r2_{a}F2_{b} + r3_{a}F3_{b} + r4_{a}F4_{b})$$

$$+ K \operatorname{space}(ri_{a}, Fi_{b}) + \sum_{n=1}^{N_{f}} ri_{a}Fi_{b}$$

$$(10)$$

where a and b take on values x, y, z to create the components of the tensor. In Eq. 10, The first term is a pairwise energy contribution where n loops over the $N_{\rm p}$ neighbors of bead i, $r_{\rm 1}$, and $r_{\rm 2}$ are the positions of the two beads in the pairwise interaction, and $F_{\rm 1}$ and $F_{\rm 2}$ are the forces on the two beads resulting from the pairwise interaction. The second term is a bond contribution of similar form for the $N_{\rm b}$ bonds which particle i is part of. There are similar



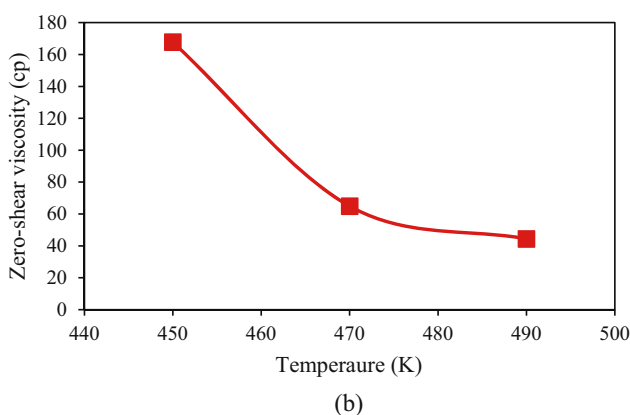


Figure 15: η_0 parameter changes in various temperatures using Green–Kubo methods for (a) PE120 and (b) PE600 matrices.

Table 6: Viscosity outputs for PE120 and PE600 matrices from the current MD simulation and previous reports

Matrix	Current simulation (cp)	Experimental reports (54) (cp)	Previous MD simulations (60) (cp)
PE120-450 K	49	14	5
PE120-470 K	30	NA	NA
PE120-490 K	24	NA	NA
PE600-450 K	168	191	18
PE600-470 K	65	NA	NA
PE600-490 K	44	NA	NA

terms for the N_a angle, N_d dihedral, and N_i improper interactions particle i is part of. There is also a term for the Kspace contribution from long-range Coulombic interactions, if defined. Eventually, there is a term for the $N_{\rm f}$ fixes that prepare internal constraint forces to bead i. The stress tensor, a mathematical representation of the internal forces within a material, is closely related to viscosity, a measure of a polymer melts resistance to deformation (23). In melts, the viscous stress tensor represents the shear stress arising from the relative motion of the melt particles. The MD outputs for η_0 are shown in Figure 15 in which viscosity decreases with temperature more considerably for PE600. Also, the viscosity of PE600 is several times higher than PE120 (53). In the designed polymeric systems, the beads' mean movement is enlarged with temperature. This thermal behavior arises from the increase in the energy of the particles with temperatures. So, the internal friction coefficient decreases, and bead–bead collisions occur with less intensity. The η_0 values are listed in Table 6 in comparison with previous simulation studies and experimental results for samples with higher weight than critical molecular weight (5,54). In experimental reports, viscosity is a function of molecular weight with $\eta = 2.1 \times 10^{-5} M_W^{1.8}$ below critical molecular weight (here PE120) and $\eta = 3.76 \times 10^{-12} M_{\rm W}^{3.64}$ (cp) above critical molecular weight (here PE600) at 450 K (54). For the validation process down for viscosity changes as a function of initial temperature, the η/η_0 parameter was calculated in the PE600 system. Numerically, this parameter reached 0.39 after 15 ns by temperature changes from 450 to 470 K. Laun et al. (57) reported between 0.3 and 0.4 for this parameter in the HDPE-based system, which has good consistency with current work. The variation of η_0 with temperature provides data to fit over the Arrhenius equation to calculate corresponding activation energy $(E_{a,vis} = \ln(\eta/\eta_0) \times R(T - T_0))$ (58). The obtained value of 0.06 and 0.1 kcal·mol⁻¹ for PE120 and PE600, respectively. According to the molecular weight of polymeric samples in our MD simulations, $E_{a,vis}$ of them varies between this parameter ratio for PE wax (59) and HDPE with high molecular weight (6) in experimental cases.

4 Conclusions

The static and dynamic properties of polymers are crucial in understanding the behavior of polymeric systems. Static properties, such as $R_{\rm g}$ and R, provide insights into the structural arrangement and stability of polymers at rest. Dynamic properties, including MSD and η_0 , reveal how polymers respond to external forces and temperature changes over time. Here, the MD approach was used to study two branched PE with 120 carbons, PE120, and 600 carbons, PE600, respectively. The former is below entanglement molecular weight, while the latter is above critical molecular weight. The simulations were performed at three initial temperatures of 450 to 490 K for 15 ns. To this purpose, R_g , R_g and C_{∞} parameters were calculated as static analysis of the equilibrated polymeric samples. Furthermore, MSD, D, and η_0 parameters were calculated to show the dynamic behavior of them. The main outputs of the modeled structures can be listed below:

- The equilibrium phase in PE120 and PE600 polymeric matrices was detected after 10 ns. Numerically, the total energy/bead of PE120 and PE600 reached to 29.860 and $32.862 \text{ kcal·mol}^{-1}$ (at $T_0 = 450 \text{ K}$). Temperature increase caused the structure evolution of these sample to intensify and the calculated energy reached 30.053 and 33.152 kcal·mol⁻¹,
- The interaction energy/bead changes inside PE120 and PE600 matrices as a function of simulation time predicted structure stability of them. The MD results showed this parameter increased to $-0.778 \,\mathrm{kcal \cdot mol}^{-1}$ between various beads of the PE600 system. Physically, this behavior arises from the mean attraction force inside the computational box.
- By $R_{\rm g}$ and R parameter analysis, the structure evolution of PE120 and PE600 matrices was estimated. The simulations indicated that the entanglements network is intensified by molecular weight. The $R_{\rm g}$ and R parameters reached 17.346 and 54.100 Å at $T_0 = 450 \,\text{K}$ in long polymeric chains.

- The MSD parameter outputs predicted that the amplitude of beads' fluctuations increases with temperature. Similarly, the molecular weight caused the beads' evolution intensity to increase. MSD parameter in the PE600 matrix converged to 54.472 Å² after 15 ns (at T_0 = 490 K). This MSD changes caused the D of PE600 polymeric samples varies from 1.5 to 2 (×10⁻⁹ m²·s⁻¹).
- The viscosity of PE120 and PE600 matrices was affected by the defined initial conditions. All simulations show this dynamic parameter decreased/increased with temperature/molecular weight. The η_0 converged to 24 cp and 44 cp in PE120 and PE600 matrices by temperature setting to 490 K. The value of this parameter increases to 49 cp and 168 cp by decreasing the temperature to 450 K.

It is expected that these MD results can optimize the static and dynamic behavior of PE-based systems in various industrial applications.

Author contributions: Amirhosein Yazdanbakhsh: methodology, investigation, modeling and simulations, writing-original draft. Ghodratollah Hashemi Motlagh: resources, review & editing.

Conflict of interest: Authors state no conflict of interest.

References

- Martín S, Expósito MT, Vega JF, Martínez-Salazar J. Microstructure and properties of branched polyethylene: application of a threephase structural model. J Appl Polym Sci. 2013;128:1871–8.
- (2) Walton KL. Metallocene catalyzed ethylene/alpha olefin copolymers used in thermoplastic elastomers. Rubber Chem Technol. 2004:77:552–68.
- (3) Tung LH. Melt Viscosity of polyethylene at zero shear. J Polym Sci. 1960;46:409–22.
- (4) Gupta BR. Polymer rheology- effect of various parameters. Rheol Appl Polym Process. 2022.
- (5) Padding JT, Briels WJ. Time and length scales of polymer melts studied by coarse-grained molecular dynamics simulations. J Chem Phys. 2002;117:925–43. doi: 10.1063/1.1481859.
- (6) Wang Roger Porter JS, Wang J, Porter RS. On the viscosity-temperature behavior of polymer melts. Rheol Acta. 1995;34:496–503.
- (7) Tschoegl NW, Knauss WG, Emri I. The effect of temperature and pressure on the mechanical properties of thermo-and/or piezorheologically simple polymeric materials in thermodynamic equilibrium-a critical review. Mech Time-Depend Mat. 2002;6:53–99.
- (8) Kourtidou D, Grigora ME, Tsongas K, Terzopoulou Z, Tzetzis D, Bikiaris DN, et al. Effect of ball milling on the mechanical properties and crystallization of graphene nanoplatelets reinforced short chain branched-polyethylene. J Appl Polym Sci. 2021;138:50874.

- (9) Baig C, Mavrantzas VG, Kröger M. Flow effects on melt structure and entanglement network of linear polymers: results from a nonequilibrium molecular dynamics simulation study of a polyethylene melt in steady shear. Macromolecules. 2010;43:6886–902. doi: 10.1021/ma100826u.
- (10) Pan Y, Bai J, Yang G, Li Z. Progress in the research on branched polymers with emphasis on the chinese petrochemical industry. Molecules. 2023;28:7934.
- (11) Lv Y, Ruan C. Molecular dynamics simulation of nonisothermal crystallization of a single polyethylene chain and short polyethylene chains based on OPLS force field. e-Polymers. 2022;22:136–46.
- (12) Guo L, Xu H, Wu N, Yuan S, Zhou L, Wang D, et al. Molecular dynamics simulation of the effect of the thermal and mechanical properties of addition liquid silicone rubber modified by carbon nanotubes with different radii. e-Polymers. 2023;23:20228105.
- (13) Salerno KM, Agrawal A, Peters BL, Perahia D, Grest GS. Dynamics in entangled polyethylene melts. Eur Phys J: Spec Top. 2016;225:1707–22. doi: 10.1140/epjst/e2016-60142-7.
- (14) Hagita K, Fujiwara S, Iwaoka N. Structure formation of a quenched single polyethylene chain with different force fields in united atom molecular dynamics simulations. AIP Adv. 2018;8:115108.
- (15) Ranganathan R, Kumar V, Brayton AL, Kroger M, Rutledge GC. Atomistic modeling of plastic deformation in semicrystalline polyethylene: role of interphase topology, entanglements, and chain dynamics. Macromolecules. 2020;53:4605–17.
- (16) Sgouros AP, Megariotis G, Theodorou DN. Slip-spring model for the linear and nonlinear viscoelastic properties of molten polyethylene derived from atomistic simulations. Macromolecules. 2017;50:4524–41.
- (17) Harmandaris VA, Mavrantzas VG, Theodorou DN. Atomistic molecular dynamics simulation of polydisperse linear polyethylene melts. Macromolecules. 1998;31:7934–43. doi: 10.1021/ma980698p.
- (18) Ramos J, Peristeras LD, Theodorou DN. Monte carlo simulation of short chain branched polyolefins in the molten state. Macromolecules. 2007;40:9640–50. doi: 10.1021/ma071615k.
- (19) Ramos J, Vega JF, Martínez-Salazar J. Molecular dynamics simulations for the description of experimental molecular conformation, melt dynamics, and phase transitions in polyethylene. Macromolecules. 2015;48:5016–27. doi: 10.1021/acs.macromol. 5b00823.
- (20) Litvinov VM, Ries ME, Baughman TW, Henke A, Matloka PP. Chain entanglements in polyethylene melts. why is it studied again? Macromolecules. 2013;46:541–7.
- (21) Martínez L, Andrade R, Birgin EG, Martínez JM. PACKMOL: a package for building initial configurations for molecular dynamics simulations. J Comput Chem. 2009;30:2157–64.
- (22) Zhang M, Lynch DT, Wanke SE. Effect of molecular structure distribution on melting and crystallization behavior of 1-butene/ ethylene copolymers. Polymer. 2001;42:3067–75.
- (23) LAMMPS molecular dynamics simulator. Available From http:// Lammps.Sandia.Gov/, 2017.
- (24) Binder K, Horbach J, Kob W, Paul W, Varnik F. Molecular dynamics simulations. J Phys: Condens Matter. 2004;16:S429.
- (25) Nath SK, Escobedo FA, de Pablo JJ. On the simulation of vapor–liquid equilibria for alkanes. J Chem Phys. 1998;108:9905–11.
- (26) Martin MG, Siepmann JI. Transferable potentials for phase equilibria. 1. united-atom description of n-alkanes. J Phys Chem B. 1998;102:2569–77.

DE GRUYTER

- Chen J-A, Chao SD. Intermolecular non-bonded interactions from machine learning datasets. Molecules. 2023;28:7900.
- (28) Wang X, Ramírez-Hinestrosa S, Dobnikar J, Frenkel D. The Lennard-Jones potential: when (not) to use it. Phys Chem Chem Phys. 2020;22:10624-33.
- (29) Toxvaerd S. Equation of state of alkanes II. J Chem Phys. 1997;107:5197-204.
- (30) Spreiter Q, Walter M. Classical molecular dynamics simulation with the velocity verlet algorithm at strong external magnetic fields. J Comput Phys. 1999;152:102-19.
- (31) Hoover WG. Canonical dynamics: equilibrium phase-space distributions. Phys Rev A. 1985;31:1695.
- (32) Behbahani AF, Vaez Allaei SM, Motlagh GH, Eslami H, Harmandaris VA. Structure, dynamics, and apparent glass transition of stereoregular poly(methyl methacrylate)/graphene interfaces through atomistic simulations. Macromolecules. 2018;51:7518-32. doi: 10.1021/acs.macromol.8b01160.
- (33) Moorthi K, Kamio K, Ramos J, Theodorou DN. Monte Carlo simulation of short chain branched polyolefins: structure and properties. Macromolecules. 2012;45:8453-66. doi: 10.1021/ ma301322v.
- (34) Tschopp MA, Bouvard JL, Ward DK, Bammann DJ, Horstemeyer MF. Influence of ensemble boundary conditions (thermostat and barostat) on the deformation of amorphous polyethylene by molecular dynamics. arXiv preprint; 2013. arXiv:1310.0728.
- Stukowski A. Visualization and analysis of atomistic simulation data with OVITO-the open visualization tool. Model Simul Mat Sci Eng. 2009:18:015012.
- (36) Alnaimi S, Elouadi B, Kamal I. Structural, thermal and morphology characteristics of low density polyethylene produced by QAPCO. Proceedings of the Proceedings of the 8th international symposium on inorganic phosphate materials. Agadir, Morocco: 2015. p. 13-9.
- (37) Brandell D, Liivat A, Aabloo A, Thomas JO. Molecular dynamics simulation of the crystalline short-chain polymer system LiPF 6 PEO 6 (M W~ 1000). J Mater Chem. 2005;15:4338-45.
- (38) Vega-Paz A, Palomeque-Santiago JF, Victorovna Likhanova N. Polymer weight determination from numerical and experimental data of the reduced viscosity of polymer in brine. Rev Mexicana de Fis. 2019:65:321-7. doi: 10.31349/REVMEXFIS.65.321.
- (39) Men Y, Rieger J, Lindner P, Enderle H-F, Lilge D, Kristen MO, et al. Structural changes and chain radius of gyration in cold-drawn polyethylene after annealing: small-and wide-angle X-ray scattering and small-angle neutron scattering studies. J Phys Chem B. 2005;109:16650-7.
- (40) Andrews J, Blaisten-Barojas E. Exploring with molecular dynamics the structural fate of PLGA oligomers in various solvents. J Phys Chem B. 2019;123:10233-44. doi: 10.1021/acs.jpcb.
- Jiang Z, Dou W, Sun T, Shen Y, Cao D. Effects of chain flexibility on the conformational behavior of a single polymer chain. J Polym Res. 2015;22:1-9.
- (42) Smith GD, Yoon DY, Jaffe RL, Colby RH, Krishnamoorti R, Fetters LJ. Conformations and structures of poly(oxyethylene) melts from molecular dynamics simulations and small-angle neutron scattering experiments. Macromolecules. 1996;29:3462-9.
- (43) Shukla GP, Bhatnagar MC. Study the synthesis parameter of tin oxide nanostructure. | Mater Sci Eng B. 2015;5:353.

- (44) Ruzette A-VG, Mayes AM. A simple free energy model for weakly interacting polymer blends. Macromolecules. 2001;34:1894-907.
- (45) Lu DR, Lee SJ, Park K. Calculation of solvation interaction energies for protein adsorption on polymer surfaces. J Biomater Sci Polym Ed. 1992;3:127-47.
- Grijpma DW, Penning JP, Pennings AJ. Chain entanglement, mechanical properties and drawability of poly (lactide). Colloid Polym Sci. 1994;272:1068-81.
- (47) Wu S. Predicting chain conformation and entanglement of polymers from chemical structure. Polym Eng Sci. 1992;32:823-30.
- Behbahani FA, Vaez Allaei SM, Motlagh HG, Eslami H, Harmandaris VA. Structure and dynamics of stereo-regular poly (methyl-methacrylate) melts through atomistic molecular dynamics simulations. Soft Matter. 2018;14:1449-64. doi: 10.1039/ c7sm02008b.
- (49) Sarmiento-Gomez E, Santamaría-Holek I, Castillo R. Mean-square displacement of particles in slightly interconnected polymer networks. J Phys Chem B. 2014;118:1146-58.
- (50) Hirata F. On the interpretation of the temperature dependence of the mean square displacement (MSD) of protein, obtained from the incoherent neutron scattering. J Mol Liq. 2018;270:218-26. doi: 10. 1016/J.MOLLIQ.2018.01.096.
- (51)Ramos J, Vega JF, Martínez-Salazar J. Assessment of entanglement features and dynamics from atomistic simulations and experiments in linear and short chain branched polyolefins. Soft Matter. 2012;8:6256-63. doi: 10.1039/c2sm25104c.
- Huster D, Schiller J, Naji L, Kaufmann J, Arnold K. NMR studies of (52)cartilage-dynamics, diffusion, degradation. Molecules in interaction with surfaces and interfaces. Berlin Heidelberg: Springer; 2004. p. 465-503.
- Padding JT, Briels WJ. Uncrossability constraints in mesoscopic polymer melt simulations: non-rouse behavior of C120H242. J Chem Phys. 2001;115:2846-59. doi: 10.1063/1.1385162.
- (54) Pearson DS, Ver Strate G, Von Meerwall E, Schilling FC. Viscosity and self-diffusion coefficient of linear polyethylene. Macromolecules. 1987;20:1133-41.
- McKenna GB. Differences in the molecular weight and the tem-(55)perature dependences of self-diffusion and zero shear viscosity in linear polyethylene and hydrogenated polybutadiene. Polymer. 1985:26:1651-3.
- (56) Pavliotis GA. Asymptotic analysis of the Green-Kubo formula. IMA J Appl Math. 2010;75:951-67.
- Laun M, Auhl D, Brummer R, Dijkstra DJ, Gabriel C, Mangnus MA, et al. Guidelines for checking performance and verifying accuracy of rotational rheometers: viscosity measurements in steady and oscillatory shear (iupac technical report). Pure Appl Chem. 2014;86:1945-68.
- (58) Santos FKG, Dantas Filho AN, Leite RHL, Aroucha EMM, Santos AG, Oliveira TA. Rheological and some physicochemical characteristics of selected floral honeys from plants of caatinga. Acad Bras Cienc. 2014;86:981-94.
- Saki TA, Sweah ZJ, Bahili MA. Effect of maleated polyethylene wax (59)on mechanical and rheological properties of ldpe/starch blends. Trop J Nat Product Res. 2021;5:1060-5. doi: 10.26538/tjnpr/v5i6.13.
- (60)Mondello M, Grest GS, Webb III EB, Peczak P. Dynamics of Nalkanes: comparison to rouse model. J Chem Phys. 1998;109:798-805.